RAA 2021 Vol. **21** No. **3**, 68(17pp) doi: 10.1088/1674-4527/21/3/68

http://www.raa-journal.org *http://iopscience.iop.org/raa*

***R**esearch in*
***A**stronomy and*
***A**strophysics*

Investigating variable stars in the open cluster NGC 1912 and its surrounding field

Chun-Yan Li (李春燕)[1,2], Ali Esamdin (艾力·伊沙木丁)[1], Yu Zhang (张余)[1], Fang-Fang Song (宋芳芳)[1,2], Xiang-Yun Zeng (曾祥云)[1,2], Li Chen (陈力)[2,3], Hu-Biao Niu (牛虎彪)[1,4], Jian-Ying Bai (白建迎)[1,2] and Jun-Hui Liu (刘军辉)[1]

[1] Xinjiang Astronomical Observatory, the Chinese Academy of Sciences, Urumqi 830011, China; *aliyi@xao.ac.cn*
[2] University of Chinese Academy of Sciences, Beijing 100049, Beijing, China
[3] Shanghai Astronomical Observatory, the Chinese Academy of Sciences, Shanghai 200030, China
[4] Department of Astronomy, Beijing Normal University, Beijing 100875, China

Received 2020 April 9; accepted 2020 September 14

Abstract In this work, we studied the variable stars in the open cluster NGC 1912 based on the photometric observations and *Gaia* DR2 data. More than 3600 CCD frames in B, V, R filters were reduced, and we obtained the light curves that span about 63 hours. By analyzing these light curves, we detected 24 variable stars, including 16 periodic variable stars, seven eclipsing binaries and one star whose type is unclear. Among these 24 variable stars, 11 are newly discovered, which are classified as six γ Doradus stars, one δ Scuti star, three detached binaries and one contact binary. We also confirmed 13 previously known variable stars. Based on cluster members identified by Cantat-Gaudin et al. (2018), we inferred cluster memberships for these detected variable stars. Using *Gaia* DR2 data, we plotted a new color-magnitude diagram for NGC 1912, and showed the nature of variable cluster members in kinematical properties and heliocentric distance. Among the 24 variable stars, seven variables are probable cluster members, which show homogeneity in kinematic characters and space position with the established cluster members. Four of the seven variable cluster members are the previously discovered stars, consisting of two γ Dor stars and two δ Sct stars. The remaining three variable cluster members, which are all γ Dor stars, are firstly detected in this work. The main physical parameters of these variable cluster members estimated from the color-magnitude diagram are $\log(\mathrm{age/yr}) = 8.75$, $[\mathrm{Fe/H}] = -0.1$, $m - M = 10.03$ mag, and $E(B - V) = 0.307$.

Key words: open clusters and associations: NGC 1912 — techniques: photometric — stars: variables: general

1 INTRODUCTION

Open clusters are ideal tracers to study the stellar populations in our Galaxy. Stars in an open cluster originated in the same interstellar cloud, so they can be assumed to have similar heliocentric distance, age, and chemical composition (Friel 1995; Piskunov et al. 2006). Searching for variable stars in the open cluster can not only verify the stellar evolution theory but also offers important clues for further understanding of the structure and the evolution of the Milky Way (Piskunov et al. 2006). However, the critical matter is to identify the membership of detected variable stars. The recent second *Gaia* data release (*Gaia* DR2) (Gaia Collaboration et al. 2018) provides a catalog of 1.3 billion sources with high precision parameter measurements to study the probable cluster memberships of stars.

The open cluster NGC 1912 [RA(J2000.0)=$05^{\mathrm{h}}28^{\mathrm{m}}40^{\mathrm{s}}$, Dec(J2000.0)=$30^{\circ}50^{'}54^{''}$] is situated in the anti-center direction of the Galaxy, in Auriga (Pandey et al. 2007). Based on photometry and spectrometry observations over the last six decades, physical properties of NGC 1912 are reliably established with its distance, reddening and age to be 1400 ± 100 pc, 0.25 ± 0.02 mag and 300 ± 80 Myr (Hoag & Applequist 1965; Subramaniam & Sagar 1999; Kharchenko et al. 2005; Pandey et al. 2007), respectively. Dias et al.

(2002a) provided a new catalog of NGC 1912 which updated the previous catalogs of Lynga (1985) and listed the membership probability of candidates based on Tycho2 proper motions (Dias et al. 2002b). Recently, Cloutier et al. (2018) identified 807 members of NGC 1912 using high-precision astrometric data from *Gaia* DR2. These members are located in an area with center ($\alpha_{J2000} = 5^{\rm h}28^{\rm m}41^{\rm s}$, $\delta_{J2000} = 35°51^{'}19^{''}$) and radius $r = 30^{'}$. Monteiro & Dias (2019) estimated the distance, reddening, and age of the cluster to be 990 ± 24 pc, 0.307 ± 0.020 mag, and $\log(\mathrm{age/yr}) = 8.538 \pm 0.0034$ from the isochrone fitting of NGC 1912 members using *Gaia* DR2 data as well.

Different types of variable stars were detected in the open cluster NGC 1912 and its surrounding field, such as Delta Scuti (δ Sct), Gamma Doradus (γ Dor), and eclipsing binaries (EBs). δ Sct stars are A- and F-type stars pulsating in p-modes with typical frequencies in the range $5-50\,\mathrm{d}^{-1}$ (Breger 2000). The p-modes in δ Sct stars are excited by the opacity mechanism operating in the He II ionization zone, as well as by turbulent pressure (Antoci et al. 2014; Xiong et al. 2016). γ Dor stars are early F-type pulsating stars with multiple periods typically between 0.4 and 3 days (Kaye et al. 1999). γ Dor stars exhibit g-modes pulsations which are excited by a convective flux modulation mechanism (Guzik et al. 2000; Dupret et al. 2005a; Grigahcène et al. 2010). EBs can be divided into Algol (EA), β Lyrae (EB) and W UMa (EW) types based on the shape of their light curves (Good 2003).

Szabó et al. (2006) detected 14 variable stars in the field of NGC 1912. There are one EW type variables, three EA type variables, five δ Sct pulsators, four long-term variable stars, and one unknown type variable star. BV photometry of the cluster were performed by Jeon (2009) in a larger field of view around the center of NGC 1912. They found 15 δ Sct stars and two γ Dor stars, and confirmed three δ Sct pulsators which were found by Szabó et al. (2006) .

Among the 20 detected variable stars, 14 variables were located within radius $30^{'}$ from the center of NGC 1912. Nevertheless, the memberships of these variable stars were not provided in the above two works. High precision parameters of these variable stars are needed to confirm their memberships for NGC 1912. For the study of variable stars, the more recently Transiting Exoplanet Survey Satellite (TESS) mission data (Ricker et al. 2015) provide new insight into pulsation stars and eclipsing binaries (e.g. Antoci et al. 2019; Gill et al. 2020).

In this paper, we present CCD time-series photometry around open cluster NGC 1912 in B, V and R bands to investigate and classify variable stars. We also infer the probable cluster memberships of detected variable stars based on *Gaia* DR2. In Section 2, we describe the target observations and data reduction. Methods we used to detect and classify variable stars and membership probabilities of the detected variable stars provided by Cantat-Gaudin et al. (2018) are presented in Section 3. In Section 4, we compared the results of this work with the previous works, showed the properties of the variable cluster members, and discussed the possibility of a variable star being another cluster member. We present a summary of results in Section 5.

2 OBSERVATIONS AND DATA REDUCTION

We observed the cluster NGC 1912 during nine nights from 2015 December 1 to 16 at the Nanshan station of the Xinjiang Astronomical Observatory. The Nanshan 1-m telescope (NOWT), equipped with an E2V CCD203-82 (4196×4096 pixels, pixel size of $12\,\mu$m), was used in our observations. The angular resolution of the telescope was $1.125^{''}$/pixel, yielding a field of view of $1.3° \times 1.3°$. An area of 2600×2400 or 2000×2000 pixels near the center of the CCD chip was read out, corresponding to a $48.75^{'} \times 45^{'}$ or $37.5^{'} \times 37.5^{'}$ field of view around the center of the cluster. The CCD operates at about $-120°$C with liquid nitrogen cooling thus the dark current is less than $1e^{-}\mathrm{pix}^{-1}h^{-1}$ at $-120°$C. The time-series observations were made using Johnson-Cousin-Bessel B, V and R filters (12s, 9s and 8s exposures respectively). In total, 1228, 1220 and 1227 CCD frames in B, V and R bands were obtained, respectively. The full observing journal is listed in Table 1.

Firstly, the CCD frames were reduced with IRAF[1], including corrections for bias level and flat field. We did not consider the dark correction since the dark current is less than $1e^{-}\mathrm{pix}^{-1}h^{-1}$ at $-120°$C. To identify objects in the CCD frames, the pixel coordinates of the frames were converted into equatorial coordinates by matching with the third US Naval Observatory CCD Astrograph Catalog (UCAC3). For the reduced CCD frames, the photometry was carried out by SExtractor[2] (Bertin & Arnouts 1996). SExtractor is a program that can perform reasonably well on astronomical images of moderately crowded star fields such as open clusters. It uses the K-σ clipping method to

[1] Image Reduction and Analysis Facility is developed and distributed by the National Optical Astronomy Observatory, which is operated by the Association of Universities for Research in Astronomy in Tucson, Arizona, USA, under operative agreement with the National Science Foundation.

[2] https://www.astromatic.net/software/sextractor

Table 1 Log of Observations Run in B, V and R Bands

Date	CCD	FOV (arcmin^2)	Length (h)	Frames B, V, R	Exposure Time B, V, R
2015 Nov 01	2600 × 2400	48.75 × 45	9	136,128,138	12,9,8
2015 Nov 02	2600 × 2400	48.75 × 45	9	156,156,154	12,9,8
2015 Nov 03	2600 × 2400	48.75 × 45	9	202,201,202	12,9,8
2015 Nov 04	2600 × 2400	48.75 × 45	5	110,111,110	12,9,8
2015 Nov 05	2600 × 2400	48.75 × 45	9	195,195,194	12,9,8
2015 Nov 07	2600 × 2400	48.75 × 45	7	153,153,153	12,9,8
2015 Nov 09	2600 × 2400	48.75 × 45	7	144,146,144	12,9,8
2015 Nov 15	2000 × 2000	37.5 × 37.5	5	78,80,79	12,9,8
2015 Nov 16	2000 × 2000	37.5 × 37.5	3	54,54,53	12,9,8

calculate the distribution of background values with the location of all small areas in CCD frames. For crowded star fields, it performs median filtering on the distribution in order to suppress possible local overestimations due to bright stars (Bertin & Arnouts 1996). Figure 1 represents the photometric errors of our observations as a function of magnitudes in B, V and R bands. As illustrated in it, the photometric errors of stars are no more than 0.05 mag in all bands when instrumental magnitudes are smaller than 19.0 mag.

Then a data processing system of XAO time-domain survey (XAO-pipeline, hereafter) was used to derive the differential light curves of stars that are brighter than 20.0 mag in instrumental magnitudes (Song et al. 2016; Ma et al. 2018). The pipeline is built based on the algorithms provided by Tamuz et al. (2005); Collier Cameron et al. (2006); Ofir et al. (2010) and the IRAF. The differential magnitude of each star is given by

$$x_{ij} = m_{ij} - \hat{m}_j - \hat{z}_i, \quad (1)$$

where m_{ij} is a two-dimensional array of instrumental magnitude, the index i denotes a single CCD frame with the entire season's data, the second index j labels an individual star. $\hat{m}_j$ is the mean instrument magnitude for each numbered star. $\hat{z}_i$ is the zero-point correction for each CCD frame (Collier Cameron et al. 2006). After repeated iterations, the differential light curves of the stars in the field of view were obtained.

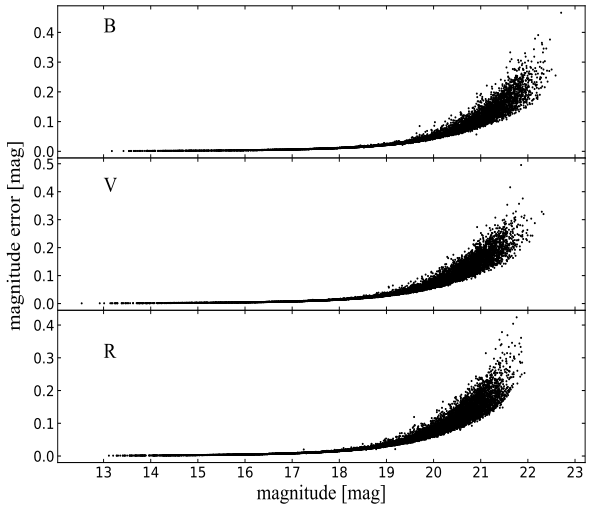

Fig. 1 Photometric errors of observations in B, V and R bands.

3 RESULTS

3.1 Detection of Variable Stars

As listed in Table 2, a total of 24 variable stars were detected in this work. The following two methods were used to search for variable stars. First, we visually inspect all the light curves to search for eclipse binaries or long-term variable stars. Stars can be considered as variable stars when their light curves show significant simultaneous variations in B, V, and R bands. Therefore, 23 variable stars with significant light curve variations were selected. We calculated the most significant periods of these stars using LombScargle periodogram (VanderPlas et al. 2012; VanderPlas & Ivezić 2015), which was achieved by the sub-package of Astropy (Astropy Collaboration et al. 2013). The folded light curves of 21 periodic stars are presented in Figures 2, 3, and 4. Figure 5 shows the light curves of V23, where we see a significant variation. However, we cannot find a reliable period to fold the light curves. To verify the long-term and small-amplitude variation of V24 detected through the XAO-pipeline, we chose a comparison star and a check star to perform differential photometry on V24. The parameters of the comparison star and the check star are listed in Table 3. Figure 6 shows their positions on the CCD frame. Figure 7 shows their differential light curves. The light curves of V24 and the comparison star are consistent with that obtained through the XAO-pipeline.

Table 2 Parameters of the Variable Stars in the Observed Field

ID	α_{2000} (deg)	δ_{2000} (deg)	V mag (mag)	A	P (d)	Type	PMemb	Discovery
V1	81.942	+36.042	16.50	0.03(2)	0.54(5)	γDor	0.8	J09
V2	81.902	+36.129	16.48	0.04(5)	0.60(8)	γDor	0.5	J09
V3	82.276	+35.577	16.42	0.02(1)	0.57(4)	γDor	0.5	this work
V4	82.057	+35.865	16.48	0.01(9)	0.45(2)	γDor	1.0	this work
V5	82.252	+35.794	16.37	0.01(6)	0.49(8)	γDor	0.8	this work
V6	81.776	+35.964	16.35	0.03(4)	0.60(5)	γDor	–	this work
V7	81.976	+36.155	15.00	0.03(3)	0.31(6)	γDor	–	this work
V8	82.065	+36.004	16.56	0.06(0)	0.20(2)	δSct	–	S06
V9	82.220	+35.985	16.05	0.01(2)	0.11(2)	δSct	–	S06
V10	81.826	+35.632	14.67	0.01(2)	0.10(7)	δSct	–	J09
V11	82.465	+36.042	15.31	0.00(6)	0.05(0)	δSct	–	J09
V12	82.514	+35.587	14.80	0.00(6)	0.05(8)	δSct	–	J09
V13	81.974	+35.764	15.88	0.00(5)	0.08(3)	δSct	–	J09
V14	82.173	+36.020	16.19	0.00(6)	0.04(6)	δSct	0.5	J09
V15	82.236	+35.939	17.87	0.03(3)	0.11(2)	δSct	–	this work
V16	82.059	+35.591	19.00	0.35(3)	0.38(4)	EW	–	S06
V17	82.012	+35.536	19.57	0.40(5)	0.34(1)	EW	–	S06
V18	81.964	+35.722	17.11	0.32(5)	0.46(6)	EW	–	S06
V19	82.299	+35.722	18.16	0.40(4)	0.38(3)	EW	–	this work
V20	81.728	+36.044	17.64	0.90(7)	2.56(6)	EA	–	this work
V21	82.250	+35.589	18.35	1.20(5)	1.24(0)	EA	–	this work
V22	82.261	+35.637	18.62	1.50(7)	0.58(9)	EA	–	this work
V23	81.830	+35.465	15.12	0.01(1)	0.56(4)	γDor	–	this work
V24	82.072	+35.820	17.49	> 0.1	–	unknown	–	S06

Column (1): variable stars' ID. Cols. (2) and (3): right ascension and declination (J2000). Col. (4): the mean instrumental magnitude of variable stars in V band, the typical uncertainties are no more than 0.05 mag. Col. (5): the amplitude of folded light curves in V band. Col. (6): the main period of variable stars calculated by LombScargle. The last-digit errors of the amplitudes and periods are given in parentheses. Col. (7): type of variable stars. Col. (8): membership probability of variable stars provided by Cantat-Gaudin et al. (2018). Col. (9): reference of variables detection. S06 and J09 indicate that the variable stars were found by Szabó et al. (2006) and Jeon (2009), respectively.

Table 3 Coordinates and Visual Magnitude of the Target, Comparison and Check Stars

Stars	α_{2000} (deg)	δ_{2000} (deg)	V (mag)	B (mag)	$B-V$ (Δ mag)
V24	82.072	+35.820	17.498 ± 0.011	18.959 ± 0.032	1.461 ± 0.023
Comparison star (C)	82.081	+35.829	15.97 ± 0.004	17.138 ± 0.007	1.168 ± 0.005
Check star (K)	82.031	+35.832	16.674 ± 0.006	17.814 ± 0.010	1.140 ± 0.008

To detect the missing periodic variable stars, we then performed frequency analyses for all other stars' time-series data in V band by using Period04 (Lenz & Breger 2004, 2005). This software adopts single-frequency Fourier and multifrequency nonlinear least-squares fitting algorithms. It offers tools to extract the individual frequencies from the multi-periodic content of time series and provides a flexible interface to perform multiple-frequency fits (Lenz & Breger 2004). The frequencies of the intrinsic and statistically significant peaks in the Fourier spectra can be extracted via iterative pre-whitening. The frequency investigations were stopped when the signal-to-noise (S/N) value is less than 4.0 (Breger et al. 1993). Amplitude spectra were computed after pre-whitening. The amplitude spectra of these stars are regarded as another criterion for finding variable stars. In this way, we detected one more variable star, whose star ID is V14. The amplitude spectrum of this variable star is shown in Figure 8. Table A.1 lists the frequency solutions, amplitudes, and S/N values of the variable star.

3.2 Cluster Membership of the Variable Stars

For variable stars detected in this work, we used the cluster members established by Cantat-Gaudin et al. (2018) to identify their membership. Cantat-Gaudin et al. (2018) used the membership assignment code Unsupervised Photometric Membership Assignment in Stellar Clusters (UPMASK) and *Gaia* DR2, and they identified 807 members of NGC 1912. Considering the precision of the data, the sources they used are $G < 18$ mag. The membership probabilities of these stars were obtained after 10 iterations of UPMASK, from 0 to 100% by an increment of 10%. Among 807 cluster members, there are 474 stars with membership probabilities over 50%. To get the cluster memberships for detected variable stars,

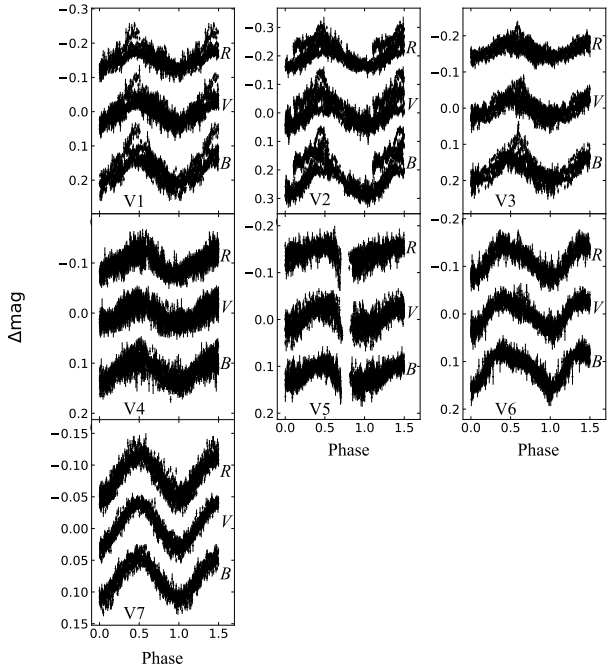

Fig. 2 R, V and B bands phase-folded light curves for star V1 to V7 listed in Table 2.

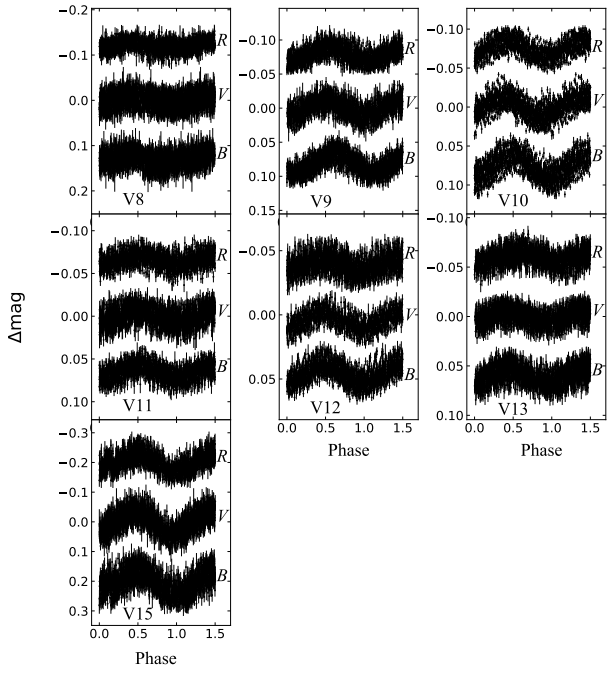

Fig. 3 Same as Fig. 2, but for star V8 to V13 and V15 listed in Table 2.

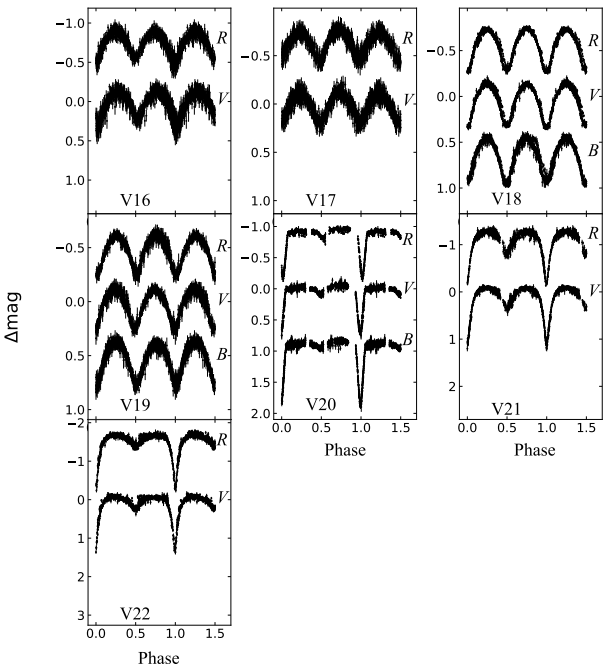

Fig. 4 Same as Fig. 2, but for star V16 to V22 listed in Table 2. The B band phase-folded light curves of V16, V17, V21 and V22 are absent because the mean instrumental magnitudes of these stars in B band are larger than 19 mag.

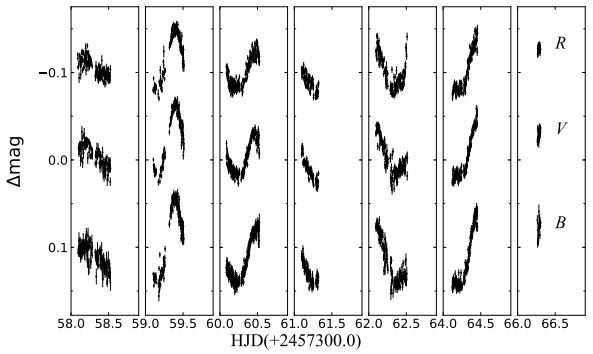

Fig. 5 Light curves of V23 in R, V and B bands.

we matched the equatorial coordinates of 2908 stars we observed with that of the 807 reported members within $3''$. As a result, 514 cluster members are detected in our field of view. Six of the 514 cluster members are variable stars studied in this work. The membership probabilities of these variable stars V1 to V5 and V14 are presented in column (8) of Table 2. All these membership probabilities are larger than 50% (see details in Table 2).

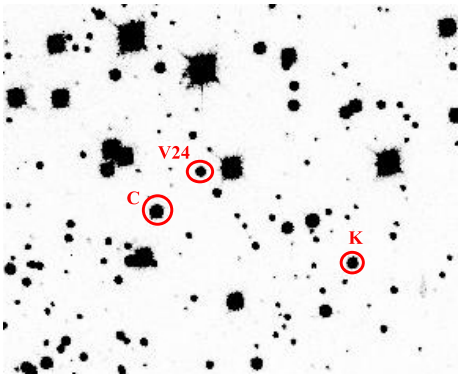

Fig. 6 V24, the comparison star and the check star are marked with red circles. They are marked with characters 'V24', 'C' and 'K' respectively.

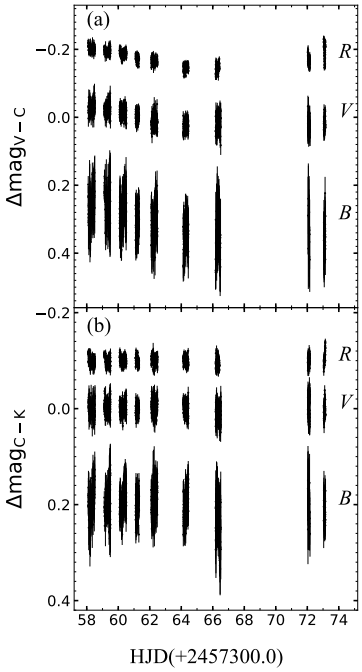

Fig. 7 Light curves of V24 in R, V and B bands. (a): Magnitude differences of V24 (V) and comparison star (C). (b): Magnitude differences of comparison (C) and check star (K).

3.3 Color-magnitude Diagram

The main physical parameters of the six variable cluster members can be estimated by an isochrone fitting of color-magnitude diagram (CMD). Figure 9 shows the isochrone fitting results for the cluster members with membership probabilities over 50%. The theoretical isochrone was derived from stellar evolutionary tracks computed with PARSEC code (Bressan et al. 2012) and its initial

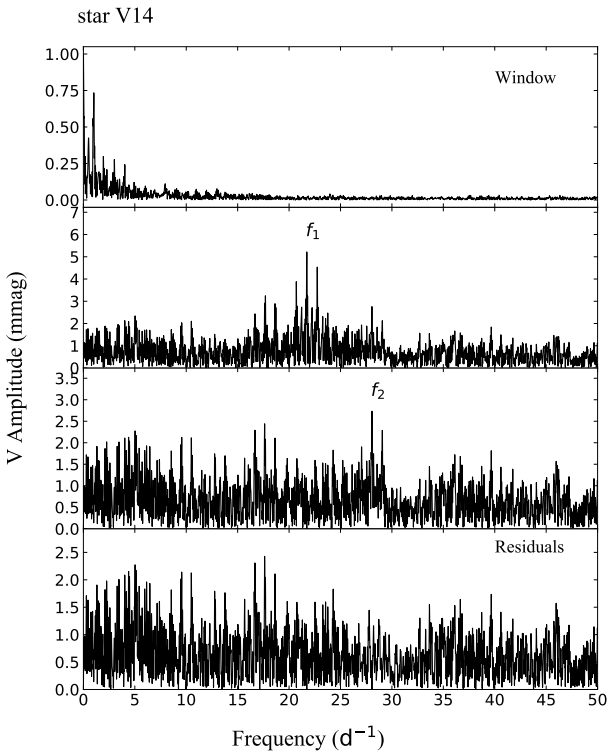

Fig. 8 Frequency analysis for star V14. The top panel: the spectral window of the light curve of V24 in V band. The sub-sequent panels: amplitude spectra of V14 with successive pre-whitening.

parameters were adopted from Monteiro & Dias (2019) and Reddy et al. (2015) for surface gravity $\log(\text{age}) = 8.75$ and metallicity $[\text{Fe/H}] = -0.1$. For each star plotted in the CMD, their observational magnitudes G mag and colors G_{BP} - G_{RP} were transformed into absolute magnitude M_G and intrinsic colors $(G_{BP} - G_{RP})_0$. We used distance modulus $m - M = 10.03$ mag, extinction $A_G = 0.841$, and colour excess $E(BP - RP) = 0.41$. The distance modulus was derived from the distance of cluster $d = 1014$ pc (Monteiro & Dias 2019). Referring to Monteiro & Dias (2019), we know that the colour excess of NGC 1912 in $B - V$ color is $E(B - V) = 0.307$. The attenuation for magnitude M_G can be calculated as:

$$A_G = R_G \times E(B - V). \quad (2)$$

The excess in G_{BP} - G_{RP} color is calculated as:

$$E(BP - RP) = (R_{BP} - R_{RP}) \times E(B - V), \quad (3)$$

where the extinction coefficients for *Gaia* filters are $R_{BP} = 3.374$, $R_{RP} = 2.035$, and $R_G = 2.740$ (Casagrande & VandenBerg 2018).

Referring to Dupret et al. (2005b,a), Aerts et al. (2010) provided an approximate range of effective temperature

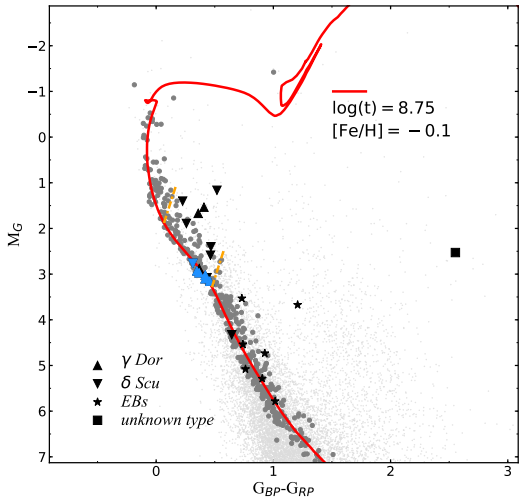

Fig. 9 CMD of NGC 1912 with isochrone and the instability strip of γ Dor stars. Grey dots represent stars with membership probabilities over 50%. The isochrone is indicated by the red line(see text for details). The approximate range of theoretical γ Dor star instability strip on the isochronous line is pointed by two orange dashed lines. Different types of variable stars are plotted with different symbols in the diagram. The corresponding legend is at the bottom left of the diagram. Blue symbols: they are variable stars detected in this work and were identified as cluster members by Cantat-Gaudin et al. (2018). Black symbols: they are variable stars but were not reported as cluster members by Cantat-Gaudin et al. (2018).

$\log T_{\rm eff}$ and $\log(L/L_\odot)$ for the instability strip of γ Dor stars, which are $\log T_{\rm eff} \in [3.83, 3.90]$ and $\log(L/L_\odot) \in [0.7, 1.1]$. We showed the instability strip of γ Dor stars in the isochrone, and plotted the 24 detected variable stars in Figure 9. These variable stars are shown as different symbols based on their types, which are identified in Section 3.2. As shown in Figure 9, the six variable members are located in the main sequence, and they are all within the instability strip of γ Dor stars that we marked.

3.4 Classification of Variable Stars

We classified the variable stars mainly by their main periods and the locations of variable cluster members in the CMD. We performed frequency analysis for the variable stars (except eclipse binaries). The corresponding frequency solutions, amplitudes, and S/N values in the V band of these stars are listed in Table A.1. The amplitude spectra of these variable stars are shown in Figure 8, Figure B.1 to Figure B.6.

We followed the criteria of Grigahcène et al. (2010) and Uytterhoeven et al. (2011) to classify these variable stars as γ Dor or δ Sct stars. The distinction between γ Dor and δ Sct stars is based completely on whether their frequencies of peaks with significant amplitudes are less or large than $5\,{\rm d}^{-1}$. From Table A.1, the dominant frequencies of V1 to V7 and V23 are less than $5\,{\rm d}^{-1}$. At the same time, the variable cluster members (V1 to V5) are located with the instability strip of γ Dor stars in the CMD of the open cluster NGC 1912. While the dominant frequencies of V8 to V15 are around or large than $5\,{\rm d}^{-1}$. We can distinguish that V1 to V7 and V23 are γ Dor stars, and V8 to V15 are δ Sct stars.

V16...V22: Figure 4 shows their folded light curves. V16, V17, V21 and V22 are too faint in B band to perform photometric analysis so that their folded light curves are empty in this band. From the shapes of these light curves and their periods, we can identify V15...V18 and V19...V21 are EW type and EA type stars respectively.

V24: From Figure 7, we can observe the long-term variabilities of light curves in three bands. The amplitude spectrum of the star is shown in Figure B.7. As listed in Table A.1, we extract two frequencies from the photometric data of V24. The main period of the star is about four days. However, the light curves of V24 show a long-term variation longer than 4 days. The position of V24 on the CMD deviates from the main sequence. Thus, the determination of the type of this variable star and the two frequencies we extracted may require more and longer observations to confirm.

4 DISCUSSION

4.1 Comparison with Previous Work

Variable stars in NGC 1912 were reported by Szabó et al. (2006) and Jeon (2009). Szabó et al. (2006) detected 14 variable stars in the field of NGC 1912 using a 60/90/180 cm Schmidt telescope with angular resolution of $1.1''$ pixel^{-1}. The 14 variables were classified as one EW type stars, three EA type stars, five δ Sct pulsators, four long-term variable stars, and one unknown type variable star by them. In a $1.0^\circ \times 1.5^\circ$ field of view around the center of NGC 1912, Jeon (2009) newly detected 15 δ Sct stars and two γ Dor stars, and they confirmed three δ Sct stars which were reported by Szabó et al. (2006). Fourteen of the 20 detected stars were located within radius $30'$ from the center of NGC 1912. The time-series CCD images for 23 nights they obtained were taken through a small refracting telescope (D = 155 mm, f = 1050 mm).

In our field of view, we observed 24 variable stars, among which 13 variable stars are previous known. Two δ Sct stars (V8, V9), three EW type stars (V16...V18) and V24 were reported by Szabó et al. (2006). Two γ Dor stars (V1 and V2) and five δ Sct stars (V10... V14) were found by Jeon (2009), and another δ Sct stars (V9) was confirmed by them. The parameters of these known variables listed in Table 2 are similar to that provided by the previous works.

Jeon (2009) performed frequency analysis on their detected pulsating stars by using Period04. The dominant frequencies of these pulsators they provided are consistent with that we list in Table A.1. However, there are some differences in other oscillation frequencies of V1, V2, V10 and V14. The second and third oscillation frequencies of V1 and V10 are different between the previous and the present work. The second and third oscillation frequencies of V1 are $1.6160 \pm 0.0022\,\mathrm{d}^{-1}$ and $1.5100 \pm 0.0026\,\mathrm{d}^{-1}$ respectively in this work, while they were $1.937\,\mathrm{d}^{-1}$ and $1.654\,\mathrm{d}^{-1}$ respectively in the previous work. The second and third oscillation frequencies of V10 are $8.4972 \pm 0.0029\,\mathrm{d}^{-1}$ and $10.6937 \pm 0.0027\,\mathrm{d}^{-1}$ in the present work, however, they are $9.7021\,\mathrm{d}^{-1}$ and $7.596\,\mathrm{d}^{-1}$ in Jeon (2009) respectively. Moreover, the frequencies we extracted from the time-series data of V10 and V14 are one more frequency than the previous work. Two frequencies of V2 were previously found, but the second oscillation frequency $2.310\,\mathrm{d}^{-1}$ cannot be identified in this work.

Apart from the 24 variable stars, we also observed 11 stars which were in Szabó et al. (2006) and Jeon (2009) but cannot be confirmed in this work. Several reasons may lead to the inconsistency. Three of the 11 stars are too faint or too bright to secure reliable variable detections in this work. Five of the 11 stars are close to nearby bright stars, it is hard for NOWT to distinguish them. For the other three stars (named C1, C2, and C3), we used the software Period 04 to perform frequency analysis on their time-series data obtained in this work. The results of the frequency analyses are listed in Table 4. Their amplitude spectra are shown in Figure 10 and Figure 11. C1 and C2 were considered to be long-term variable stars by Szabó et al. (2006), but the possible periods of these stars were not given. In this study, the extracted frequency of C1 is $0.9522 \pm 0.0027\,\mathrm{d}^{-1}$. We detected two independent frequencies from the observation data of C2, which are $0.9091 \pm 0.0015\,\mathrm{d}^{-1}$ and $0.5109 \pm 0.0021\,\mathrm{d}^{-1}$. The corresponding periods are one day and two days within 1σ error, respectively. However, observations in this work are affected by the interruption of daytime, we cannot determine whether these periodic signals are caused by the stars' intrinsic variation or the interval of our observations.

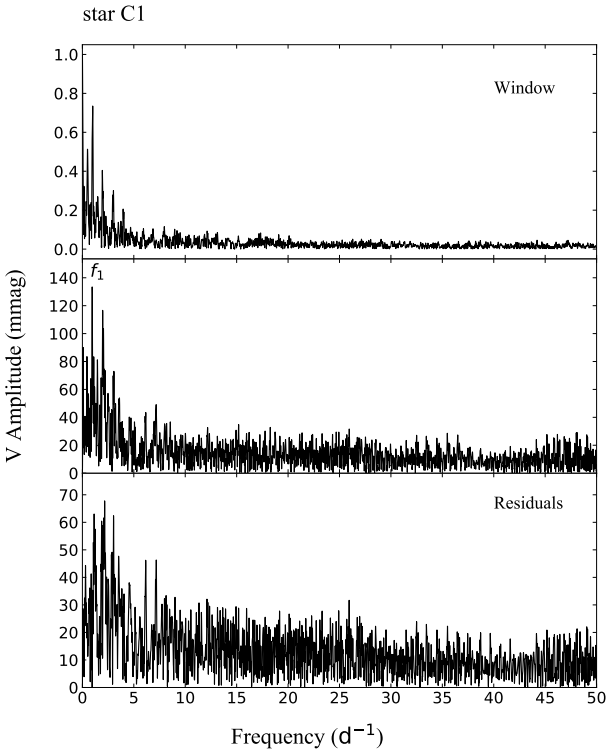

Fig. 10 The same as Fig. 8 but for star C1.

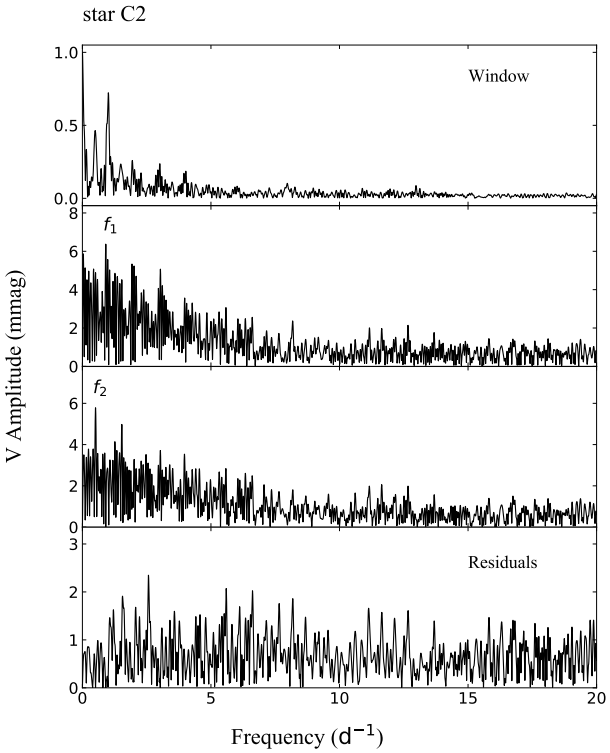

Fig. 11 The same as Fig. 8 but for star C2.

Table 4 Frequency Solutions for Three Previous Known Variable Stars

star ID	α_{2000} (deg)	δ_{2000} (deg)	No.	F_{19} (c/d)	A_{19} (mag)	S/N_{19}
C1	81.9772	35.8637	f_1	0.9522 ± 0.0027	0.1334 ± 0.0099	6.6
C2	82.2203	35.5810	f_1	0.9091 ± 0.0015	0.0063 ± 0.0004	14.0
			f_2	0.5109 ± 0.0021	0.0057 ± 0.0004	10.0
C3	82.2532	35.8946	–	–	–	< 4.0

The same as Table A.1 but for three previous known variable stars C1 to C3.

Since the peaks in the amplitude spectrum of C3 are lower than four times the noise level, we do not show its amplitude spectrum. Additional precise observations may be required to further study these variable stars.

Otherwise, variables observed by the previous work are outside our field of view. They are not taken into account in this section.

4.2 Parameters of Variable Cluster Members

Variable stars V1 to V5 and V14 were reported by Cantat-Gaudin et al. (2018) as cluster members of NGC 1912, since they concentrated within the field of NGC 1912 on the sky and are homogeneous with the other members in proper motions and parallaxes. Figure 12 demonstrates the homogeneousness of these variable cluster members in celestial position (α, δ), proper motion ($\mu_{\alpha*}$, μ_δ), and parallax (ω). As shown in panel (a) of Figure 12, these variable stars are located in the field with center ($\alpha = 5^{\rm h}28^{\rm m}42.7^{\rm s}$, $\delta = 35^\circ51'32''$) and radius $r = 30'$. The field covers the field of NGC 1912 reported by Pandey et al. (2007), center in ($\alpha = 5^{\rm h}28^{\rm m}43^{\rm s}$, $\delta = 35^\circ51'18''$) with $r \backsim 14'$. Cluster members perform uniform bulk motions, they will be over-density in the proper motion diagram. In panel (b) of Figure 12, we see that the members of NGC 1912 cluster together showing different proper motions with the other stars. The six variable stars perform uniform bulk motions with the members, since their proper motion values are similar to the proper motion of NGC 1912 reported by Dias et al. (2014) ($\mu_{\alpha*} = -0.52 \pm 1.44$ mas yr^{-1} and $\mu_\delta = -4.14 \pm 1.54$ mas yr^{-1}). As we can see in panel (c) of Figure 12, the histogram of parallax for these cluster members is fitted with a Gaussian distribution, $\mu = 0.86$ mas, $\sigma = 0.08$ mas. The typical uncertainties in parallax are $0.02 - 0.1$ mas for stars brighter than $G = 18$ mag (Gaia Collaboration et al. 2018). The parallaxes of these variable members are shown as blue dots, and they are less than 2σ of the Gaussian distribution. Values of these parallaxes are in good agreement with that of NGC 1912 provided by Monteiro & Dias (2019) (0.874 ± 0.064 mas).

Among these variable cluster members, V2 is the only one that was observed by the Large Sky Area Multi-Object Fibre Spectroscopic Telescope (LAMOST) (Cui et al. 2012; Zhao et al. 2012). Figure 13 shows the LAMOST DR5 (Luo et al. 2015) spectrum of V2. Note that the relative flux calibration was performed for the spectrum (Song et al. 2012), and there are no units for flux values. The stellar parameters are $T_{\rm eff} = 7190 \pm 120$ K, $\log(g) = 4.2 \pm 0.2$, $[{\rm Fe/H}] = -0.3 \pm 0.1$ and heliocentric radial velocity $R_v = -5 \pm 10$ km s^{-1}. The parameters of V2 are in good agreement with that of γ Dor stars in literature. Considering that V1...V5 and V14 were identified as cluster members with membership probabilities large than 50% by Cantat-Gaudin et al. (2018), the parameters of the other variable members should be very likely similar to that of V2.

These 24 detected variable stars are listed in the input catalog of TESS, but the observation data of these variable stars have not been released.

4.3 Another Probable Variable Cluster Member

Among the 24 variable stars we detected, six variables were reported as the cluster members of NGC 1912 by Cantat-Gaudin et al. (2018). Apart from these six variable cluster members, there is one variable star that seems to be another variable cluster member, which is V10. It is a variable star in the field of NGC 1912 and exhibits a similar motion with the cluster members whose membership probabilities are larger than 0.9.

As shown in panel (a) and panel (c) of Figure 12, V10 is located within the field of the open cluster. The parallax of V10 is $\omega_{V10} = 1.0644 \pm 0.044$ mas , which is between 2 and 2.5 σ of the cluster's parallax distribution.

From kinematic information, we may get more hints about the membership of V10. Since there are no radial velocity measurements for the cluster members and detected variables in *Gaia* DR2, we can use proper motion parameters to perform the kinematic analysis only. The cluster members and detected variables are all brighter than $G = 18$ mag, corresponding to typical uncertainties 0.3 mas yr^{-1} in proper motion (Cantat-Gaudin et al. 2018). As shown in panel (b) of Figure 12, V10 shows a similar proper motion with the variable cluster members. Panel (d) of Figure 12 shows the spatial distributions

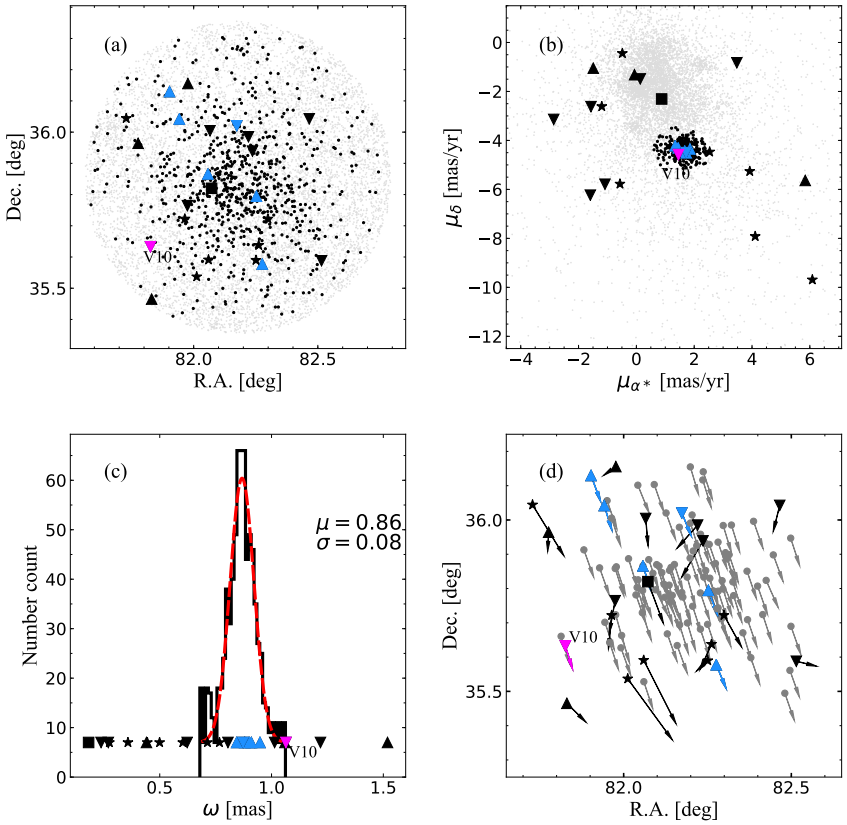

Fig. 12 (a): Spatial distribution for the cluster members and detected variable stars, (α_{J2000} δ_{J2000}). (b): proper motion distribution for the cluster members and detected variable stars. (c): A histogram of parallax (ω) for cluster members (black line) and variable stars obtained in this work. The histogram of the members' parallax can be fitted with a single Gaussian profile(red dashed line). (d): Spatial distribution for the cluster members and detected variable stars with their tangential velocities. Arrows point out the direction of tangential velocities for each star. Arrow length is in proportion to the tangential speed. In top panels, light grey dots mean the complete samples of NGC 1912. Black dots represent all cluster members established by Cantat-Gaudin et al. (2018). The meanings of the rest marks are identical to that in Figure 9 but magenta symbol means the probable variable cluster member in Section 4.3. The grey dots in panel (d) represent stars with membership probabilities over 90%.

and corresponding tangential velocities of the detected variable stars and the cluster members with membership probabilities over 90%. The distances of these stars were estimated by Bailer-Jones et al. (2018). Thus, we can calculate their tangential velocities (V_t) from their proper motions and distances:

$$V_t = 4.74 \times \mu \times d\,, \tag{4}$$

where μ is the proper motion in arcsec yr^{-1}, d is the distance in parsecs, V_t is the tangential velocity in km s^{-1}. For the cluster members, their tangential velocities range from 6.82 km s^{-1} to 12.05 km s^{-1} in RA, and -28.16 km s^{-1} to –24.24 km s^{-1} in Dec. As demonstrated in panel (d) of Figure 12, the magnitude and direction of the tangential velocity of V10 are almost the same as that of the cluster members whose membership probabilities are larger than 90%.

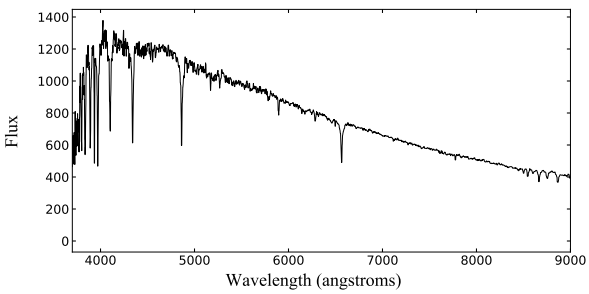

Fig. 13 Spectrum of V2.

It is possible that V10 is the another cluster member. However, more observations are needed to determine the membership of V10.

5 SUMMARY

We investigated and characterized the variable stars in the open cluster NGC 1912 and its surrounding field by photometric observations. We detected 24 variable stars from nine nights photometric observations. We also referred the cluster members established by Cantat-Gaudin et al. (2018) and *Gaia* DR2 to obtain the membership probability and the physical parameters of these detected variable stars. Six variable cluster members were found. A new CMD was constructed based on the cluster members with membership probabilities over 50%.

We classified the detected variable stars according to their main periods and the positions of the variable cluster members on the CMD. We discovered six γ Dor stars, one δ Sct star, one EW type star, and three EA type stars. We also confirmed 13 variable stars detected by Szabó et al. (2006) and Jeon (2009), consisting of two γ Dor stars, seven δ Sct stars, three EW type stars, and one unknown type variable star. For the unknown type variable star, its spectrogram and light curves show that it may be a long-term variable star. More observations are needed to determine its period. In the future, the more TESS data released will help us further understand the variable stars in the open cluster NGC 1912.

In addition to the six variable members reported by Cantat-Gaudin et al. (2018), we potentially find a new cluster member candidate. It can be confirmed by the homogeneity of the position and kinematics of the star with the identified cluster members. We determined the main physical parameters of these variable cluster members by a fitting of isochrone. The best fitting shows $\log(\mathrm{age/yr}) = 8.75$, $[\mathrm{Fe/H}] = -0.1$, $m - M = 10.03$ mag, and $E(B-V) = 0.307$. These parameters are very similar to that of NGC 1912 provided by Monteiro & Dias (2019).

Acknowledgements The authors acknowledge the National Natural Science Foundation of China under grants 11873081 and 11661161016, 2017 Heaven Lake Hundred-Talent Program of Xinjiang Uygur Autonomous Region of China, and the program of Tianshan Youth (No. 2017Q091). The CCD photometric data of NGC 1912 were obtained with the Nanshan 1 m telescope of Xinjiang Astronomical Observatory. This work has made use of data from the European Space Agency (ESA) mission *Gaia* (https://www.cosmos.esa.int/web/gaia), processed by the *Gaia* Data Processing and Analysis Consortium (DPAC, https://www.cosmos.esa.int/web/gaia/dpac/consortium). Funding for the DPAC has been provided by national institutions, in particular the institutions participating in the *Gaia* Multilateral Agreement. The Guo Shou Jing Telescope (the Large Sky Area Multi-Object Fiber Spectroscopic Telescope LAMOST) is a National Major Scientific Project built by the Chinese Academy of Sciences. Funding for the project has been provided by the National Development and Reform Commission. LAMOST is operated and managed by the National Astronomical Observatories, Chinese Academy of Sciences.

Appendix A: THE RESULTS OF FREQUENCY ANALYSIS FOR PERIOD VARIABLE STARS

Appendix B: THE AMPLITUDE SPECTRA OF PERIOD VARIABLE STARS

References

Aerts, C., Christensen-Dalsgaard, J., & Kurtz, D. W. 2010, Asteroseismology (Springer Science+Business Media)
Antoci, V., Cunha, M., Houdek, G., et al. 2014, ApJ, 796, 118
Antoci, V., Cunha, M. S., Bowman, D. M., et al. 2019, MNRAS, 490, 4040
Astropy Collaboration, Robitaille, T. P., Tollerud, E. J., et al. 2013, A&A, 558, A33
Bailer-Jones, C. A. L., Rybizki, J., Fouesneau, M., Mantelet, G., & Andrae, R. 2018, AJ, 156, 58
Bertin, E., & Arnouts, S. 1996, A&AS, 117, 393
Breger, M. 2000, in Astronomical Society of the Pacific Conference Series, 210, Delta Scuti and Related Stars, eds. M. Breger & M. Montgomery, 3
Breger, M., Stich, J., Garrido, R., et al. 1993, A&A, 271, 482
Bressan, A., Marigo, P., Girardi, L., et al. 2012, MNRAS, 427, 127
Cantat-Gaudin, T., Jordi, C., Vallenari, A., et al. 2018, A&A, 618, A93
Casagrande, L., & VandenBerg, D. A. 2018, MNRAS, 479, L102
Cloutier, R., Doyon, R., Bouchy, F., & Hébrard, G. 2018, AJ, 156, 82
Collier Cameron, A., Pollacco, D., Street, R. A., et al. 2006, MNRAS, 373, 799
Cui, X.-Q., Zhao, Y.-H., Chu, Y.-Q., et al. 2012, RAA (Research in Astronomy and Astrophysics), 12, 1197
Dias, W. S., Alessi, B. S., Moitinho, A., & Lépine, J. R. D. 2002a, A&A, 389, 871
Dias, W. S., Lépine, J. R. D., & Alessi, B. S. 2002b, A&A, 388, 168
Dias, W. S., Monteiro, H., Caetano, T. C., et al. 2014, A&A, 564, A79

Table A.1 Frequency Solutions for Periodic Variable Stars

star ID	No.	F_{19} (c/d)	A_{19} (mag)	S/N_{19}	F_{09} (c/d)
V1	f_1	1.8350 ± 0.0007	0.0313 ± 0.0006	16.2	1.823
	f_2	1.6160 ± 0.0022	0.0123 ± 0.0007	7.7	1.937
	f_3	1.5100 ± 0.0026	0.0056 ± 0.0008	4.8	1.654
V2	f_1	1.6432 ± 0.0006	0.0448 ± 0.0007	8.4	1.644
	f_2	–	–	–	2.310
V3	f_1	1.7428 ± 0.0019	0.0203 ± 0.0005	23.9	–
	f_2	2.6259 ± 0.0059	0.0065 ± 0.0005	6.4	–
	f_3	1.8922 ± 0.0041	0.0065 ± 0.0005	8.6	–
V4	f_1	2.2130 ± 0.0008	0.0191 ± 0.0004	14	–
	f_2	2.4386 ± 0.0018	0.0082 ± 0.0004	6.5	–
V5	f_1	2.0076 ± 0.0031	0.0154 ± 0.0006	8.2	–
	f_2	1.8948 ± 0.0048	0.0052 ± 0.0006	4.4	–
V6	f_1	1.6526 ± 0.0005	0.0331 ± 0.0004	40.1	–
	f_2	3.3152 ± 0.0027	0.0059 ± 0.0004	11.5	–
V7	f_1	3.1553 ± 0.0003	0.0324 ± 0.0003	36.1	–
	f_2	0.06967 ± 0.0018	0.0041 ± 0.0003	5.3	–
	f_3	4.7281 ± 0.0036	0.0030 ± 0.0003	4.8	–
V8	f_1	4.9512 ± 0.0032	0.0056 ± 0.0004	7.4	–
	f_2	0.3716 ± 0.0051	0.0040 ± 0.0004	4.7	–
V9	f_1	8.8854 ± 0.0014	0.0109 ± 0.0005	18.0	8.878
	f_2	0.8958 ± 0.0042	0.0054 ± 0.0005	8.6	–
	f_3	8.3712 ± 0.0041	0.0046 ± 0.0005	8.1	–
	f_4	0.3086 ± 0.0047	0.0036 ± 0.0006	7.9	–
	f_5	8.6299 ± 0.0059	0.0035 ± 0.0004	4.8	–
V10	f_1	9.2986 ± 0.0015	0.0121 ± 0.0003	13.5	9.301
	f_2	8.4972 ± 0.0029	0.0069 ± 0.0003	8.1	9.702
	f_3	10.6937 ± 0.0027	0.0049 ± 0.0003	5.8	7.596
	f_4	6.0452 ± 0.0041	0.0046 ± 0.0003	4.6	–
V11	f_1	19.9574 ± 0.0031	0.0063 ± 0.0048	8.1	19.965
	f_2	3.2151 ± 0.0064	0.0042 ± 0.0049	5.2	–
	f_3	2.0417 ± 0.0055	0.0034 ± 0.0057	5.0	–
	f_4	4.0578 ± 0.0067	0.0026 ± 0.0052	4.8	–
V12	f_1	17.1571 ± 0.0014	0.0060 ± 0.0002	26.8	17.152
	f_2	0.7970 ± 0.0045	0.0018 ± 0.0002	5.1	–
	f_3	15.0934 ± 0.0063	0.0014 ± 0.0002	4.7	–
	f_4	19.5135 ± 0.0088	0.0010 ± 0.0002	5.1	–
V13	f_1	11.9810 ± 0.0019	0.0049 ± 0.0002	16.9	11.980
	f_2	15.2229 ± 0.0037	0.0027 ± 0.0002	5.7	–
	f_3	1.9792 ± 0.0041	0.0027 ± 0.0002	4.3	–
	f_4	12.8618 ± 0.0049	0.0020 ± 0.0002	4.8	–
V14	f_1	21.7225 ± 0.0035	0.0052 ± 0.0004	7.6	21.719
	f_2	28.0563 ± 0.0062	0.0027 ± 0.0004	4.6	–
V15	f_1	8.9683 ± 0.0013	0.0323 ± 0.0010	22.1	–
	f_2	16.1318 ± 0.0038	0.0114 ± 0.0010	5.5	–
	f_3	6.9378 ± 0.0029	0.0108 ± 0.0010	9.5	–
	f_4	0.0630 ± 0.0021	0.00980.0010	16.4	–
	f_5	0.8029 ± 0.0037	0.00790.0010	9.3	–
	f_6	8.6233 ± 0.0050	0.00720.0010	5.4	–
V23	f_1	1.7732 ± 0.0062	0.0253 ± 0.0006	47.8	–
	f_2	2.0048 ± 0.0049	0.0112 ± 0.0006	41.9	–
	f_3	1.4685 ± 0.0084	0.0107 ± 0.0011	32.9	–
	f_4	1.1273 ± 0.0066	0.0065 ± 0.0008	25.3	–
	f_5	2.3582 ± 0.0099	0.0061 ± 0.0008	13.5	–
	f_6	3.5769 ± 0.0077	0.0039 ± 0.0004	7.7	–
	f_7	3.9039 ± 0.0012	0.0033 ± 0.0005	5.4	–
	f_8	4.3081 ± 0.0023	0.0027 ± 0.0005	5.9	–
	f_9	0.3290 ± 0.0087	0.0021 ± 0.0017	6.4	–
V24	f_1	0.2587 ± 0.0035	0.0057 ± 0.0005	5.9	–
	f_2	2.5747 ± 0.0048	0.0037 ± 0.0005	5.2	–

For each star, only independent frequencies are listed. The uncertainty of frequencies were calculated by the error matrix of the least-squares using Period04. A represents amplitude of frequency peaks in Fourier spectrum. The subscripts of 09 and 19 mean that the Fourier analysis results of these variable stars are derived by Jeon (2009) and this work, respectively.

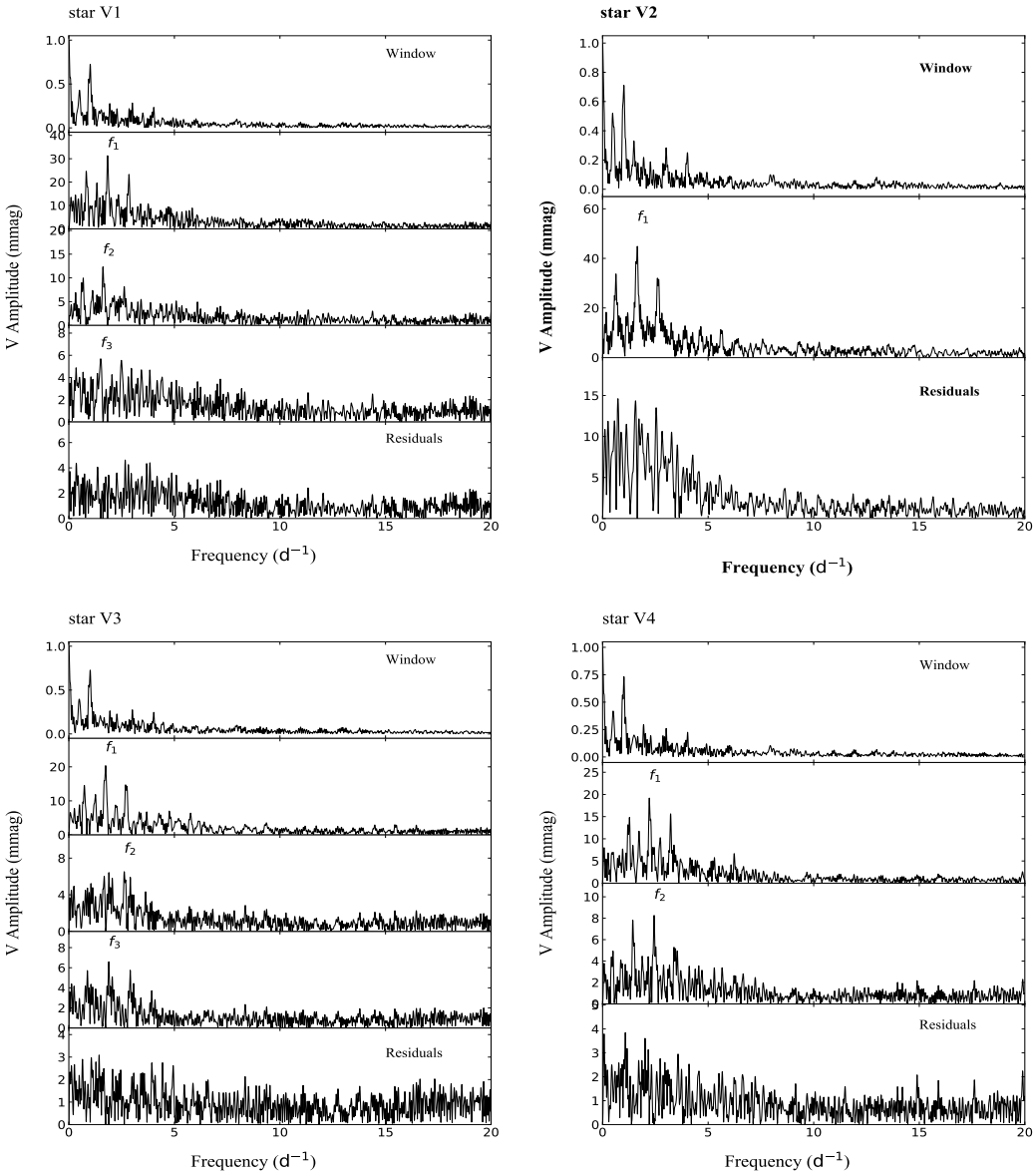

Fig. B.1 The same as Fig. 8 but for star V1 to V4.

Dupret, M. A., Grigahcène, A., Garrido, R., et al. 2005a, MNRAS, 360, 1143
Dupret, M. A., Grigahcène, A., Garrido, R., Gabriel, M., & Scuflaire, R. 2005b, A&A, 435, 927
Friel, E. D. 1995, ARA&A, 33, 381
Gaia Collaboration, Brown, A. G. A., Vallenari, A., et al. 2018, A&A, 616, A1
Gill, S., Cooke, B. F., Bayliss, D., et al. 2020, MNRAS, 495, 2713
Good, G. A. 2003, Observing Variable Stars
Grigahcène, A., Antoci, V., Balona, L., et al. 2010, ApJL, 713, L192
Guzik, J. A., Kaye, A. B., Bradley, P. A., Cox, A. N., & Neuforge, C. 2000, ApJL, 542, L57
Hoag, A. A., & Applequist, N. L. 1965, ApJS, 12, 215
Jeon, Y. B. 2009, Publication of Korean Astronomical Society, 24, 9
Kaye, A. B., Handler, G., Krisciunas, K., Poretti, E., & Zerbi, F. M. 1999, PASP, 111, 840
Kharchenko, N. V., Piskunov, A. E., Röser, S., Schilbach, E., & Scholz, R. D. 2005, A&A, 438, 1163
Lenz, P., & Breger, M. 2004, in IAU Symposium, 224, The A-Star Puzzle, eds. J. Zverko, J. Ziznovsky, S. J. Adelman, & W. W. Weiss, 786
Lenz, P., & Breger, M. 2005, Communications in Asteroseismology, 146, 53
Luo, A. L., Zhao, Y.-H., Zhao, G., et al. 2015, RAA (Research in Astronomy and Astrophysics), 15, 1095

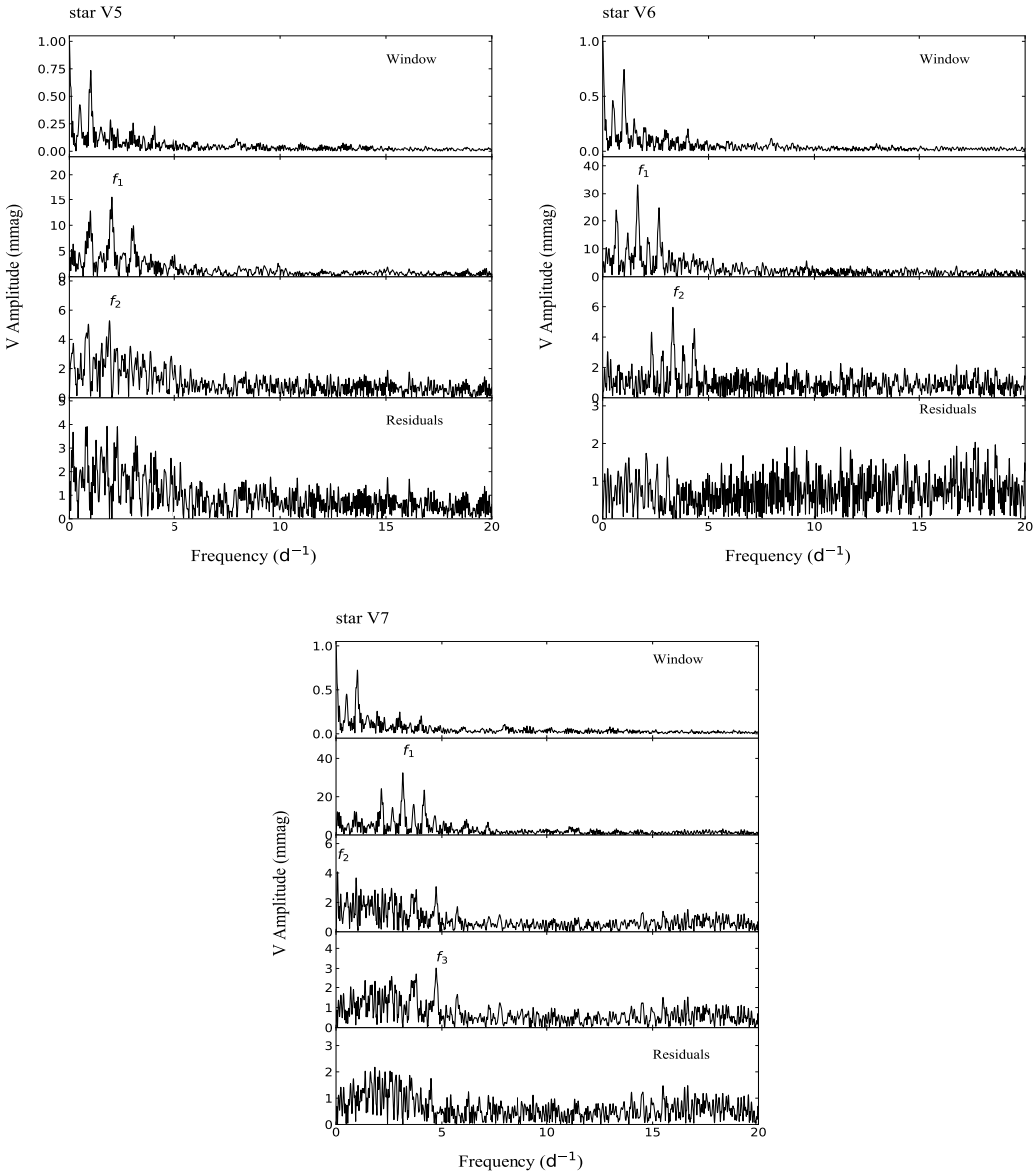

Fig. B.2 The same as Fig. 8 but for star V5 to V7.

Lynga, G. 1985, in IAU Symposium, Vol. 106, The Milky Way Galaxy, eds. H. van Woerden, R. J. Allen, & W. B. Burton, 143
Ma, S.-G., Esamdin, A., Ma, L., et al. 2018, Ap&SS, 363, 68
Monteiro, H., & Dias, W. S. 2019, MNRAS, 487, 2385
Ofir, A., Alonso, R., Bonomo, A. S., et al. 2010, MNRAS, 404, L99
Pandey, A. K., Sharma, S., Upadhyay, K., et al. 2007, PASJ, 59, 547
Piskunov, A. E., Kharchenko, N. V., Röser, S., Schilbach, E., & Scholz, R. D. 2006, A&A, 445, 545
Reddy, A. B. S., Giridhar, S., & Lambert, D. L. 2015, MNRAS, 450, 4301
Ricker, G. R., Winn, J. N., Vanderspek, R., et al. 2015, Journal of Astronomical Telescopes, Instruments, and Systems, 1, 014003
Song, F.-F., Esamdin, A., Ma, L., et al. 2016, RAA (Research in Astronomy and Astrophysics), 16, 154
Song, Y.-H., Luo, A. L., Comte, G., et al. 2012, RAA (Research in Astronomy and Astrophysics), 12, 453
Subramaniam, A., & Sagar, R. 1999, AJ, 117, 937
Szabó, G. M., Furész, G., Székely, P., & Szentgyorgyi, A. 2006, in Astronomical Society of the Pacific Conference Series, 349, Astrophysics of Variable Stars, eds. C. Aerts & C. Sterken, 339
Tamuz, O., Mazeh, T., & Zucker, S. 2005, MNRAS, 356, 1466
Uytterhoeven, K., Moya, A., Grigahcène, A., et al. 2011, A&A, 534, A125
VanderPlas, J., Connolly, A. J., Ivezic, Z., & Gray, A. 2012, in Proceedings of Conference on Intelligent Data Understanding

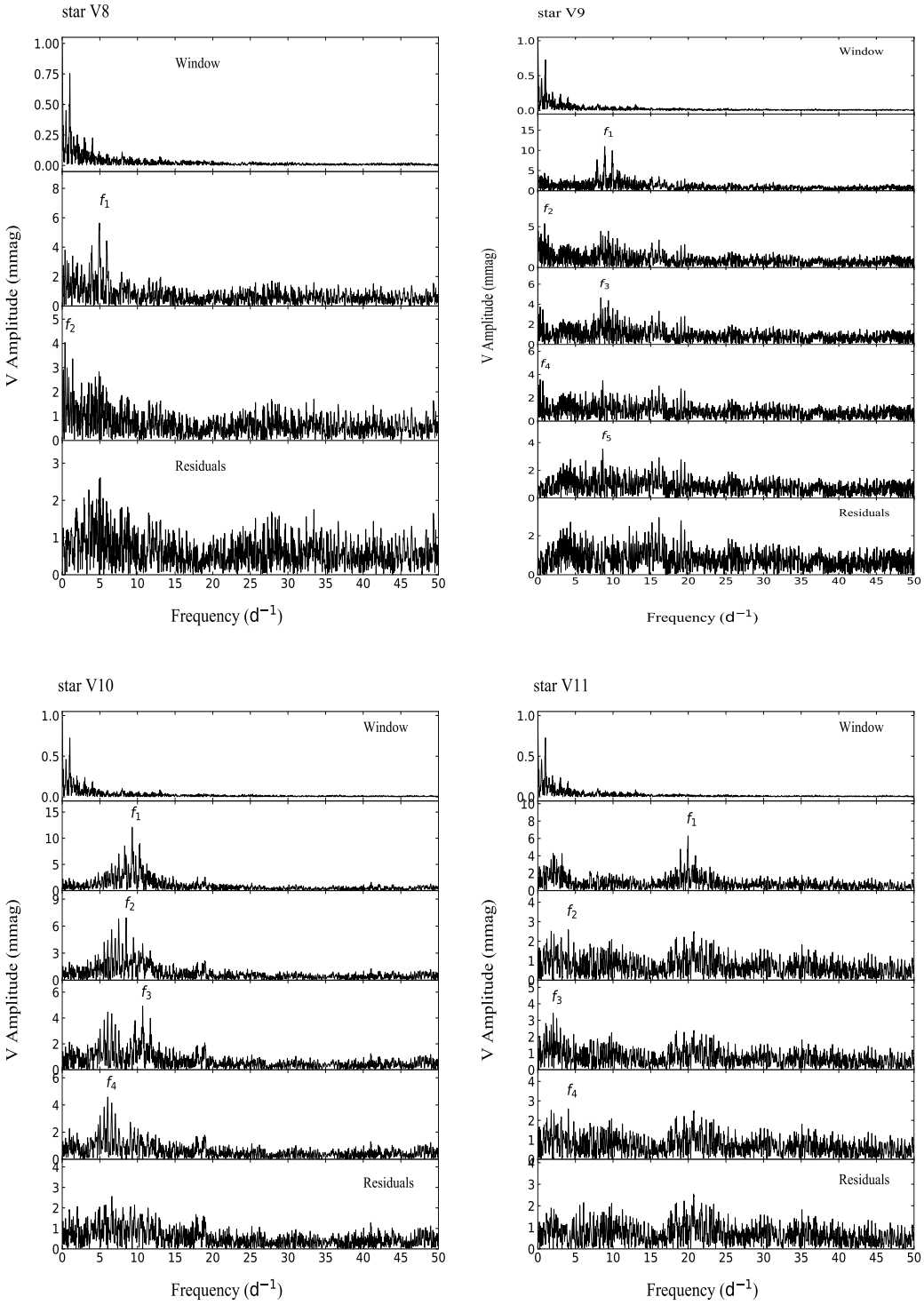

Fig. B.3 The same as Fig. 8 but for star V8 to V11.

(CIDU), 47
VanderPlas, J. T., & Ivezić, Ž. 2015, ApJ, 812, 18
Xiong, D. R., Deng, L., Zhang, C., & Wang, K. 2016, MNRAS, 457, 3163
Zhao, G., Zhao, Y.-H., Chu, Y.-Q., Jing, Y.-P., & Deng, L.-C. 2012, RAA (Research in Astronomy and Astrophysics), 12, 723

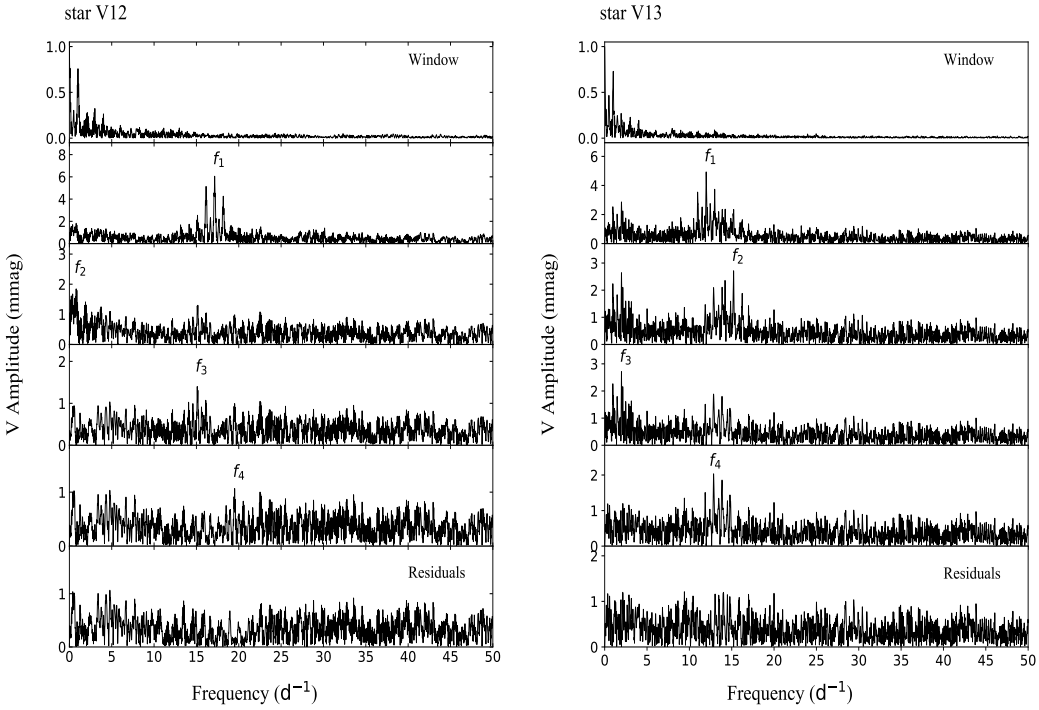

Fig. B.4 The same as Fig. 8 but for star V12 and V13.

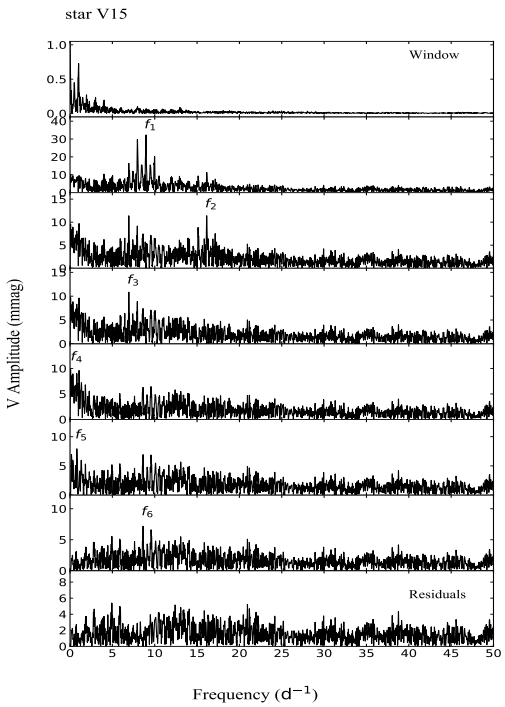

Fig. B.5 The same as Fig. 8 but for star V15.

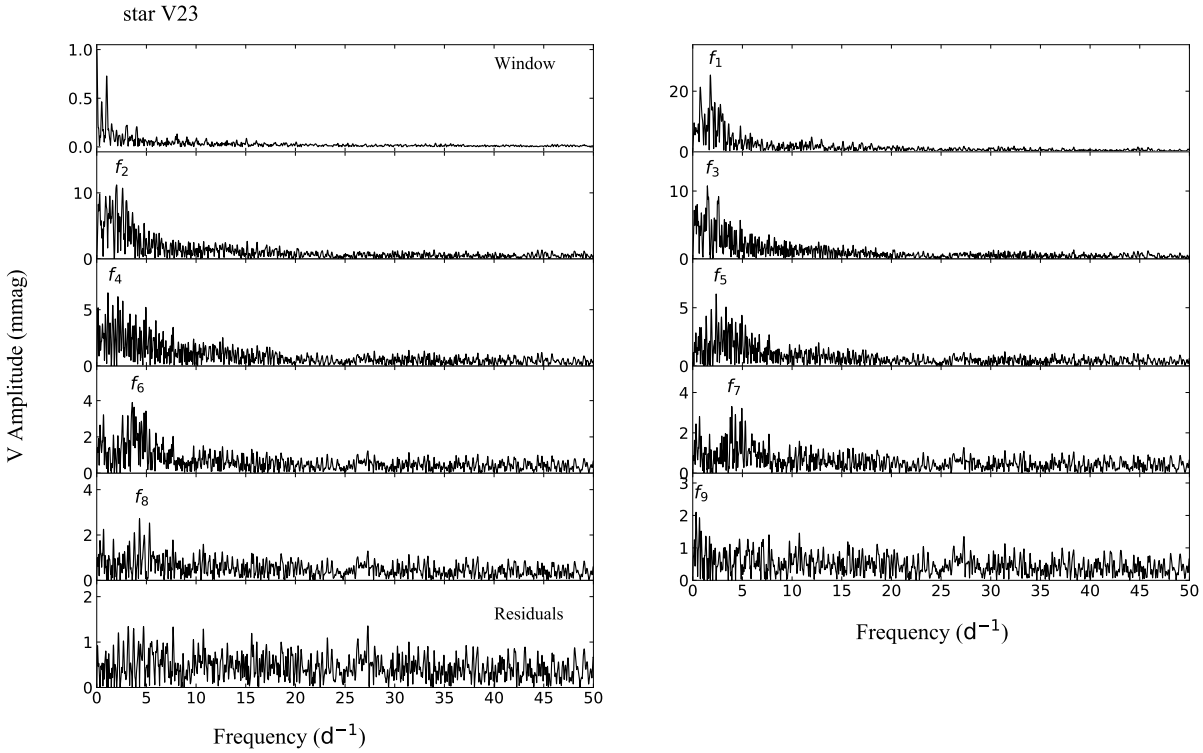

Fig. B.6 The same as Fig. 8 but for star V23.

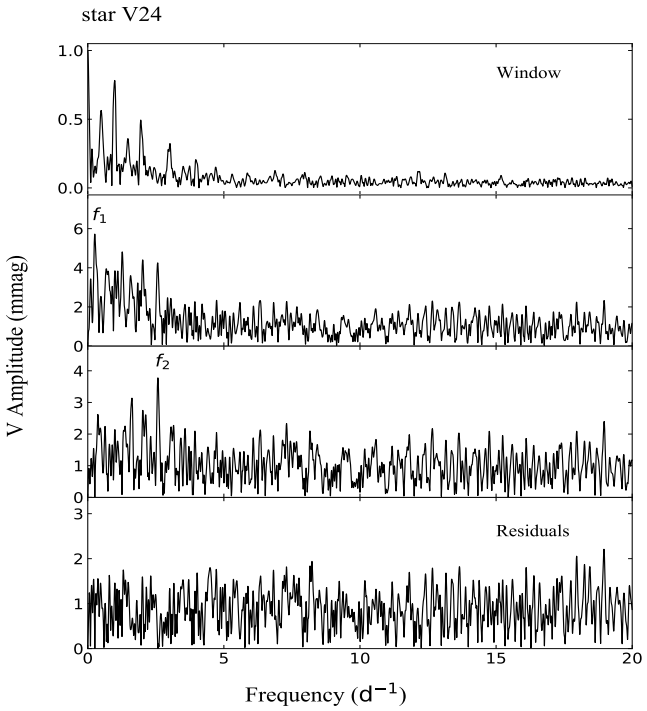

Fig. B.7 The same as Fig. 8 but for star V24.